Detiding Three-Dimensional Velocity Survey Data in Coastal Waters*

ANDREAS MÜNCHOW

Institute of Marine and Coastal Sciences, Rutgers–The State University of New Jersey, New Brunswick, New Jersey

(Manuscript received 9 October 1998, in final form 8 July 1999)

ABSTRACT

A three-dimensional data interpolation technique is proposed that efficiently removes tidal currents from spatial velocity surveys. The least squares method extends prior two-dimensional detiding methods to three spatial dimensions using biharmonic splines. Biharmonic splines are fitted to velocity data from acoustic Doppler current profiler (ADCP) surveys, moorings, and ocean surface current radar (OSCR). The data are used to predict diurnal and semidiurnal tidal currents on the inner shelf off New Jersey that vary between 1 and 15 cm s^{-1} at spatial scales of about 20 km. The (tidal) signal to (subtidal) noise is thus $O(1)$ in the study area. Although the main task of this study is to remove tidal variance from the ADCP survey data, an attempt is made to accurately ''predict'' tidal currents from the data. The latter task is more difficult. Both artificial data with known signal-to-noise properties and actual measurements indicate that the method estimates both diurnal and semidiurnal tidal currents to within about 3.5 cm s^{-1} rms, or 30% of the true tidal signals. While the biharmonic splines remove tidal currents successfully, the prediction of the vertical structure of tidal currents is only fair. Some experimentation guided by physical intuition and prior knowledge of the tidal fields is necessary in order to obtain an accurate and stable solution. While this ambiguity constitutes the main disadvantage of the method, its simple algebraic expression to predict tidal currents in space and time is its main advantage. Properly weighting velocity data from different sources, such as moorings, surface current radar, and ADCP surveys of different quality, improves the quality of the fit.

1. Introduction

During the last decade, acoustic Doppler current profilers (ADCPs) have become routine instruments to measure ocean currents in both vertical and horizontal dimensions. Using one of the first vessel-mounted ADCPs, Joyce and Stalcup (1984) reported on Gulf Stream rings. Kosro and Huyer (1986) pioneered their use in the coastal ocean when they studied upwelling filaments off California with a vessel-mounted ADCP system. Kaneko et al. (1990) used a towed ADCP system to obtain synoptic velocity profiles of the Kuroshio Current off Japan. Poor navigation and compass data represented early challenges to obtain absolute velocity measurements from a moving platform. Calibration algorithms were suggested by Joyce (1989) and Münchow et al. (1995) for vessel-mounted and towed ADCP systems, respectively. The removal of tidal currents from ADCP survey data remains a main challenge. This is particularly true in coastal applications where both tidal currents and their spatial gradients can be large.

Tidal currents constitute a major signal on many continental shelves that alias velocity observations from a moving ship. While tidal sea level oscillations generally are well observed, most recently from altimeters (Ray and Mitchum 1996), the spatial distribution of tidal currents is largely unknown, especially where the bottom topography changes at small spatial scales, such as in the coastal ocean. In order to resolve the topographic effects of tidal current variability, Geyer and Signell (1990) designed ADCP surveys to describe such flows near a coastal headland. Generally, however, tidal currents constitute a nuisance that often severely limits the ability to interpret ADCP data. Hence, methods were developed to remove the tidal component of the velocity record. Candela et al. (1992), Foreman and Freeland (1991), and Münchow et al. (1992a) devised methods to remove tidal currents from ADCP survey data. Candela et al. (1992) considered depth-averaged tidal currents only when they used polynomials and biharmonic splines to find semidiurnal and diurnal tidal currents off China and Brazil. Foreman and Freeland (1991) experimented with a barotropic numerical model of the tides off Vancouver Island, Canada, where the diurnal tidal wave has properties of a topographic vorticity wave. Münchow et al. (1992a) considered tidal currents to vary

* Institute of Marine and Coastal Sciences Contribution Number 98-29.

Corresponding author address: Dr. Andreas Münchow, The Graduate College of Marine Studies, University of Delaware, Robinson Hall, Newark, DE 19716-3501.
E-mail: andreas@udel.edu

along a single section using polynomials and Ekman layer solutions in the horizontal and vertical, respectively. Allen (1995) first applied these methods to ADCP velocities collected in the open ocean using data from extensive surveys and a 15-day-long current meter mooring. More recently, Dowd and Thompson (1996) and Bogden and O'Donnell (1998) introduced barotropic data assimilation techniques to solve the problem of detiding ADCP survey data. All of these methods, however, were strictly two dimensional. In contrast, Steger et al. (1998) fits tidal currents that vary in all three spatial dimensions. They prescribe the tidal velocity field to vary linearly with latitude, longitude, and depth in the Gulf of Farallones off California. In this paper, I extend the previous work by Candela et al. (1992) to three spatial dimensions using biharmonic splines. These allow more flexibility in the functional character of the tidal currents than do first-order polynomials. Also, for three-dimensional biharmonic splines, the number of coefficients to be determined by the method of least squares is the same as it is for two-dimensional biharmonic splines. In contrast, polynomials require additional parameters to account for vertical variability that increase rapidly with the order of the polynomial.

2. Study area and data sources

Figure 1 depicts the study area off New Jersey that extends from the coast to the 25-m isobath about 30 km offshore. Figure 1 also shows the location of current measurements using moorings (Fig. 1b), shore-based radar (Fig. 1c), and shipborne ADCP surveys (Fig. 1d). The water depths at these measurement locations are always less than 30 m. Numerous shoals and banks extend 2–4 m above the generally sandy sea floor.

During the summer of 1996, seven current meter moorings were deployed from May through August inshore of the 25-m isobath (Fig. 1b). Along the central line (C line), ADCPs at locations C1, C2, and C3 measured currents at vertical intervals of 1 m or better, within about 4 m of the surface. Moorings at the southern locations S1 and S3 contained two and three S4 current meters, respectively, in water 12 and 25 m deep. In the north, inshore at N1, three S4 current meters measured the flow in 10-m-deep water, while offshore, at N3, an ADCP profiled the 25-m-deep water column in 1-m vertical bins. Münchow and Chant (2000) describe processing details of these moorings and the subtidal temperature and current fields. The National Ocean Service (NOS) deployed two moorings in 1984 in the study area. Their locations are shown in Fig. 1b and are labeled 24 and 25. I will use these data herein for an independent verification of the method. The mooring data used in this study represent averages sampled at 3-h intervals.

As part of a larger experiment on the dynamics of wind-driven motions on a shallow, stratified shelf, 6-day-long surveys of the velocity field were conducted,

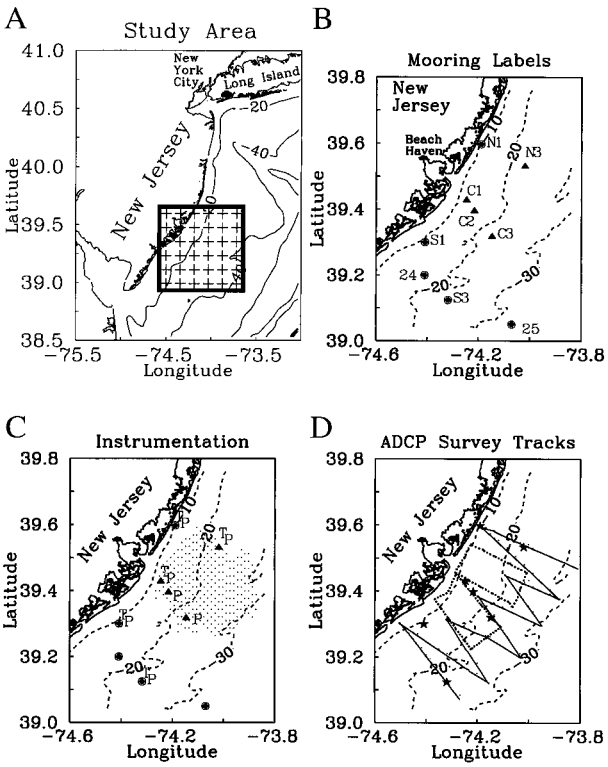

FIG. 1. Maps of the study area. (a) Large-scale view with grid of the study area. (b) The 1996 mooring locations of electromagnetic current meters at locations N1, S1, and S3 (circles); upward-looking ADCPs at N3, C1, C2, and C3 (triangles); as well as two 1984 mooring locations at 24 and 25. (c) The OSCR measurement locations overlaid with symbols for mooring locations with additional sensors (*t*, temperature; *p*, pressure). (d) The ship tracks of ADCP surveys of the R/V *Cape Henlopen* (thick solid line) and the M/V *NorthStar4* (dotted line). Contours indicate the bottom topography in (a) 20-m intervals and [(b), (c), (d)] 10-m intervals.

with two ships, on the inner shelf off New Jersey in June, July, and August 1996. The R/V *Cape Henlopen* contained a hull-mounted 1228-kHz narrowband ADCP that was calibrated following the procedure of Joyce (1989): that is, the transducer misalignment and scaling coefficients were 59.0° and 1.0232, respectively. The M/V *NorthStar4* towed an Endeco V-fin tow body that housed both a 1228-kHz broadband ADCP and a conductivity–temperature–depth (CTD) recorder at a depth of 2–4 m, depending on sea state. Münchow et al. (1995) describe a similar tow system, its performance off California and Alaska, and necessary compass calibration of the data it returns. Both systems profile the velocity field continuously in all three spatial dimensions and track the bottom at all times. Table 1 lists details of the instrument setup, random errors, and calibration coefficients for both systems. Figure 2 compares the vessel's velocity over ground as determined from bottom-tracking ADCP and navigational global position system (GPS) data after calibration at times when the ship sailed at steady speed along a straight course. The agreement is excellent relative to similar applications of the tow

TABLE 1. ADCP details. The abbreviations NB and BB refer to narrowband and broadband instruments. The three experiments in June, July, and August 1996 are referred to as 9606, 9607, and 9608. The R/V *Cape Henlopen* contains a vessel-mounted ADCP inside a sea chest, while the M/V *NorthStar4* deployed a subsurface ENDECO tow body that housed a direct-reading ADCP.

	R/V *Cape Henlopen*	M/V *NorthStar4*
ADCP type and frequency	NB—1228 kHz	BB—1228 kHz
Beam angle	30°	20°
Ping rate	0.25 Hz	0.5 Hz
Pings/ensemble (preprocessing)	4	4
Vertical bin size	1.0 m	0.5 m
Transducer depth	1.0 m	2–4 m
Blanking	1.0 m	0.5 m
Time average (postprocessing)	5 min	2 min
Nominal accuracy (random error)	0.4 cm s^{-1}	0.3 cm s^{-1}
rms BT–GPS (calibration, Fig. 2)	2.7 cm s^{-1}	8.8 cm s^{-1}
Navigation	DGPS	GPS
Calibration: (a) scaling 9606, 9607, 9608	1.02321	0.99191, 0.99756, 1.00010
Calibration: (b) misalignment, 9606, 9607, 9608	59.0°	187.9°, 191.5°, 187.9°
Calibration: (c) cos(heading)	n/a	−3.5°

system (Münchow et al 1995): root-mean-square (rms) discrepancies between the bottom-tracking pulse and GPS-determined ship speeds are about 2.7 and 8.8 cm s^{-1} for the vessel-mounted (R/V *Cape Henlopen*) and towed (M/V *NorthStar4*) ADCPs, respectively (Table 1). The discrepancies reflect poor navigational rather than poor ADCP data. Differential GPS and long transect lines explain the smaller rms discrepancy for the vessel-mounted ADCP. In contrast, the towed system relied on ordinary GPS and short transect lines. Both towed and vessel-mounted ADCPs always tracked the bottom, and errors common to the water- and bottom-tracking pulses are minimized since earth-referenced velocities are the difference of velocities derived from bottom- and water-tracking pulses.

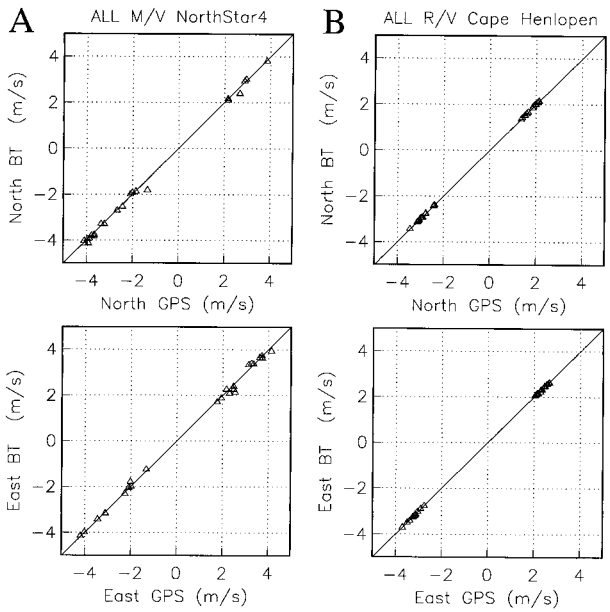

FIG. 2. Final calibration curves for (a) the towed ADCP of the M/V *NorthStar4* and (b) the vessel-mounted ADCP of the R/V *Cape Henlopen*. The labels GPS and BT refer to velocities determined from the navigational global position system and the bottom tracking of the ADCPs.

Figure 1d shows a typical survey pattern of the two-ship surveys. These were repeated up to four times during each 6-day survey. The towed ADCP system surveyed daily about four sections that each extended about 15–20 km across the shelf. Along these sections the tow system collected velocity profile data in 0.5-m vertical bins at a rate of about four pings per ensemble every 3 s. Subsequently, these data are screened and processed to result in quality-controlled, calibrated data that are averaged 2 min along the ship track if the ship's speed exceeded 3 m s^{-1}. This eliminates data of generally poor quality during acceleration, deceleration, and frequent station work. Underway speeds varied between 3.5 and 4.5 m s^{-1}. A 2-min temporal average resolves currents at a spatial scale of about 500 m.

The 1996 experiment also employed an ocean surface current radar (OSCR) to measure surface currents over a spatial domain in 1×1 km^2 spatial bins. The range of OSCR measurements varied between 0 and 40 km across the shelf as a function of sea state and, more importantly, as a function of the intensity of nearby electromagnetic disturbances associated with a poorly shielded municipal power line. Figure 1c shows the optimal OSCR coverage in the northern and central part of the study area. Chant and Münchow (1999, manuscript submitted to *J. Phys. Oceanogr.*) describe both operating details and calibration to moored ADCP data for the 1996 application off New Jersey. Graber et al. (1997) discuss comprehensively overall performance of OSCR to measure surface currents. Intercomparison studies generally conclude with rms accuracies of about 6–8 cm s^{-1}.

3. Tidal current variability

Four parameters describe a tidal ellipse. These are the major (RMAJ) axis inclined by an angle ORIE from true east, a minor (RMIN) axis, and a current phase

TABLE 2. Tidal coefficients at NOS moorings 24 and 25 from Münchow et al. (1992b). Three instruments were Grundy 9021G current meters that were deployed in 1984/85. The record length *T*, water depth *H*, instrument depth *z*, and semimajor amplitudes (RMAJ) for M_2, K_1, O_1, and N_2 are shown.

Latitude	Longitude	*T* (days)	*H* (m)	*z* (m)	M_2 (cm s^{-1})	K_1 (cm s^{-1})	O_1 (cm s^{-1})	N_2 (cm s^{-1})
39°12.0′	74°24.8′	229	18	7	7.9	2.8	2.7	1.8
		156		10	7.5	2.6	3.0	1.5
		156		15	5.6	2.6	2.3	1.5
39°03.1′	74°04.3′	84	31	8	9.6	2.4	3.7	1.4
		108		15	11.2	2.7	3.0	3.1
		154		27	8.6	1.3	1.6	2.4

(PHASE). Münchow et al. (1992b) define these four parameters in detail in a study of tidal currents off New Jersey, Delaware, and Maryland using a collection of data from historical current meter moorings. Two of these moorings were deployed near the present study area (see Fig. 1b for location of moorings 24 and 25), and each contained three current meters in water 18 and 31 m deep. Table 2 indicates that semidiurnal tidal currents near the bottom varied from 5 to 9 cm s^{-1}, while near the surface, they varied between 7 and 11 cm s^{-1}. Diurnal currents were generally smaller, about 2–3 cm s^{-1}. It appears as if tidal currents vary little with depth and across the shelf. However, this false appearance results from poor vertical resolution.

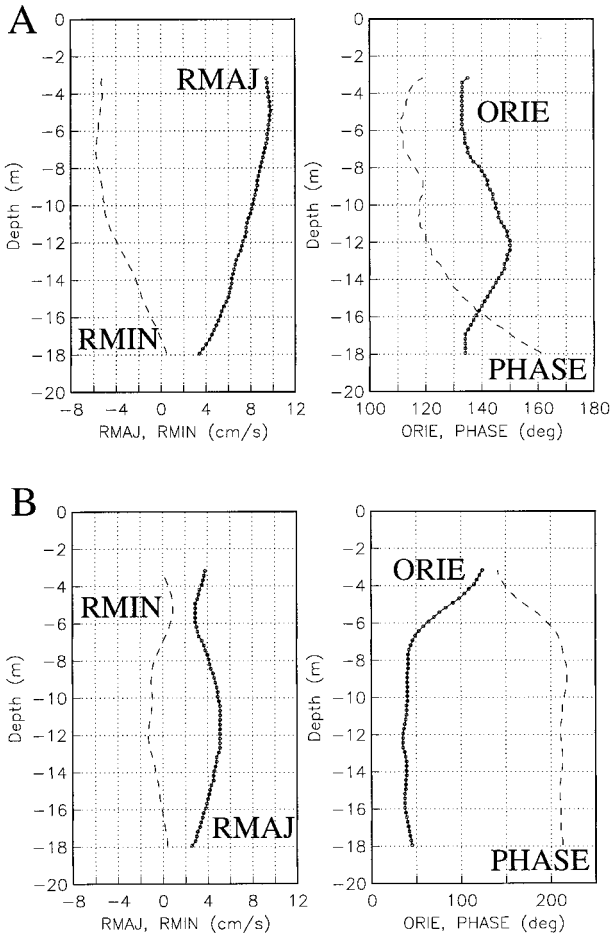

FIG. 3. Tidal ellipse properties at the central mooring location C2 for (a) the semidiurnal M_2 and (b) the diurnal K_1 tidal currents. Note the different scales for the M_2 and K_1 tidal ellipse parameters. A negative semiminor (RMIN) axis refers to clockwise rotation of currents on the ellipse. RMAJ, RMIN, ORIE, and PHASE refer to the semimajor axis, semiminor axis, semimajor axis orientation, and current phase, respectively. Symbols on the curves labeled RMAJ and ORIE indicate ADCP bin locations at 0.5-m vertical intervals.

Figure 3 shows vertical profiles of ellipse parameters for C2 at the very center of the study area. The semidiurnal M_2 tidal current has an amplitude that varies from less than 4 cm s^{-1} near the bottom to 10 cm s^{-1} near the surface (Fig. 3a). The negative sign of RMIN indicates that tidal currents rotate clockwise except near the bottom, where the flow is almost rectilinear (RMIN = 0). Near the surface, RMAJ and RMIN reach 10 and 5 cm s^{-1}, respectively, and thus, the ratio of minor to major axis is about 0.5. The major axis veers about 20° within about 6 m off the bottom (ORIE), while the phase angle changes by more than 30° over the same vertical distance. This implies that maximum tidal currents occur about an hour earlier near the bottom than they do near the surface. Similar results are found in tidal flows influenced by bottom friction (Maas and Van Haren 1987; Prandle 1982; Münchow et al. 1992a).

The diurnal K_1 tidal currents at C2 are weaker. However, they are still sizable, as their amplitude RMAJ exceeds 5 cm s^{-1} at a middepth maximum about 12 m below the sea surface (Fig. 3b). The K_1 tidal ellipse is nearly rectilinear, as the ratio RMIN/RMAJ rarely exceeds 0.25. The orientation of the major axis veers almost 90° within 6 m of the surface. Furthermore, the almost rectilinear K_1 tidal currents during the study period exhibit a distinct subsurface amplitude maximum of about 5 cm s^{-1} at middepth (Fig. 3b) that, as is shown herein, is well resolved by the least squares solutions. The enhanced diurnal currents are found near a sharp summer pycnocline (not shown). Chant and Münchow (1999, manuscript submitted to *J. Phys. Oceanogr.*) discuss inertial oscillations that are trapped near the pycnocline within the study area in 1996. The physical exploration of diurnal internal waves is beyond the scope of this study. However, the potential of internal waves to contribute to the vertical variability of tidal

currents favors the use of biharmonic splines rather than polynomials as spatial base functions.

4. Biharmonic splines

Sandwell (1987) elegantly and concisely derives details of biharmonic spline interpolation that he applies to satellite altimetry data in two dimensions. Biharmonic splines satisfy the biharmonic equation

$$\nabla^4 w(\mathbf{x}) = \sum_{j=1}^{N} \alpha_j \delta(\mathbf{x} - \mathbf{x}_j), \tag{1}$$

where ∇^4 is the biharmonic operator, $\mathbf{x}$ represents a location in a space of m dimensions, δ is the Dirac delta function, and "j" indicates N data (Sandwell 1987). The solutions to this equation are biharmonic Green's function $\phi_m(\mathbf{x})$: that is,

$$w(\mathbf{x}_i) = \sum_{k=1}^{K} \alpha_k \phi_m(\mathbf{x}_i - \mathbf{x}_k), \tag{2}$$

which in two ($m = 2$) and three ($m = 3$) dimensions has the forms

$$\phi_2(\mathbf{x}) = |\mathbf{x}|^2 \cdot (\ln|\mathbf{x}| - 1) \quad \text{and} \tag{3}$$

$$\phi_3(\mathbf{x}) = |\mathbf{x}|, \tag{4}$$

where $\mathbf{x} = \mathbf{x}_i - \mathbf{x}_k$ and $i = 1, 2, \ldots, N$ represent data, while $k = 1, 2, \ldots, K$ represents specified nodal locations. Both K and the nodal locations $\boldsymbol{x}_k$ are arbitrary (as long as $\mathbf{x}_k \neq \mathbf{x}_i$). That is, for $K \ll N$, solutions can be fitted by using the method of least squares (Candela et al. 1992). In order to remove tidal currents $u = u(x, y, z, t)$ in three spatial dimensions, $\mathbf{x} = (x, y, z)$ and time t, I thus propose to fit velocity observations u_i to the "model"

$$u(x, y, z, t) = \sum_{k=1}^{K} \sum_{j=1}^{M} \{[\alpha_{jk} \cos(\omega_j t) + \beta_{jk} \sin(\omega_j t)] \times \phi_3(x, y, z, x_{jk}, y_{jk}, z_{jk})\}, \tag{5}$$

where

$$\phi_3(x, y, z, x_{jk}, y_{jk}, z_{jk}) = [(x - x_{jk})^2 + (y - y_{jk})^2 + (z - z_{jk})^2]^{1/2}, \tag{6}$$

and the index j represents a tidal constituent with a frequency ω_j. The analyst needs to specify the number and the locations of the nodes $(x, y, z)_{jk}$ for each tidal constituent. The constant parameters α_{jk} and β_{jk} are to be determined by the method of weighted least squares (Press et al. 1992). That is, the squared deviation χ^2

$$\chi^2 = \chi^2(\alpha_{jk}, \beta_{jk}) = \sum_{i=1}^{N} \left(\frac{u_i - u(\alpha_{jk}, \beta_{jk})}{\sigma_i} \right)^2 \tag{7}$$

will be minimized with respect to the unknowns α_{jk} and β_{jk}, given the observations u_i and the predictions $u(\alpha_{jk}, \beta_{jk})$ defined in (5) and (6). The minimization

$$\frac{\partial \chi^2(\alpha_{jk}, \beta_{jk})}{\partial(\alpha_{jk}, \beta_{jk})} = 0 \tag{8}$$

results in a set of $2KM$ linear equations for each velocity component. The observations are subject to an error σ_i that must be specified a priori. The errors represent weights given to individual data. Most published ADCP detiding algorithms use $\sigma_i = 1$. However, it will be shown herein that assigning different weights to velocity data from different sources improves the statistical fit. Allen (1995) weighted ADCP survey data by the water depth in order to emphasize observations over shoaling topography.

Note that the order of the fit defined as the number of fitted parameters α_{jk} and β_{jk} for each tidal constituent j depends only on the number of nodal locations K. The order of the fit does not increase with using the biharmonic splines in two [(3)] or three [(4)] spatial dimensions. The order of the fit increases only with the number of nodes K and tidal constituents M. In contrast, polynomials such as those used by Steger et al. (1998) always require additional coefficients even for a linear fit in three spatial dimensions. Furthermore, first-order polynomials require 16 parameters for each tidal constituent, while biharmonic splines require only 4 parameters for every node for every constitutent. Thus, linear polynomials are of the same "order" as a biharmonic spline fit with four nodes. The main drawback of biharmonic spline interpolation is the sensitivity of the solutions to the location of the nodes. Furthermore, along with all other least squares methods, biharmonic spline interpolation lacks a physical basis. However, the method ensures smooth fields, since it is mathematically equivalent to the constraint of minimum curvature in a variational approach to data interpolation (McIntosh 1990). Initial experiments and promising results reveal the efficient and successful removal of tidal currents from a large dataset. The implementation of the method straightforwardly extends results from two to three spatial dimensions, which is an advantage for code development. While I do not claim superiority of this method over others, it does constitute the first attempt to remove tidal currents in three spatial dimensions using biharmonic splines. The method promises to reduce tidal variance of baroclinic, frictional, and barotropic motions from ADCP surveys. Using linear polynomials in three dimensions, Steger et al. (1998) find their fits to reveal largely barotropic tidal currents that are little affected by frictional forces.

5. Testing and sensitivity

Three-dimensional biharmonic spline interpolation techniques have not been applied to oceanographic velocity datasets previously. It is thus prudent to test, using artificial data, both the method and its sensitivity to changing parameters. Subsequent sections will verify the method against mooring observations off New Jer-

sey and an application to an ADCP survey conducted in August 1996. The result will be a thoroughly tested algorithm that predicts tidal currents to within about 4 cm s^{-1} rms. In order to resolve the neap–spring cycle, it will be necessary to use properly weighted data from a variety of sources.

a. Simulated velocity fields

For testing purposes, an artificial velocity field is specified as

$$u(x, y, z, t) = 10(y + 1 - z)(\cos(\omega_{m2}t) + 0.5 \sin(\omega_{k1}t)) + N(0, 15) \quad \text{and} \tag{9}$$

$$v(x, y, z, t) = N(0, 15), \tag{10}$$

where (x, y, z) are scaled spatial coordinates that represent longitude, latitude, and depth, respectively, while ω_{m2} and ω_{k1} represent, respectively, the frequency of the semidiurnal M_2 and diurnal K_1 tidal constituents that have periods of 12.42 and 23.93 h. For the study area off New Jersey (Fig. 1), the horizontal coordinates (x, y) are scaled by 63 km, while the vertical coordinate is scaled by the local water depth. The scaling ensures that (x, y, z) vary in the interval [0, 1]. A Gaussian noise component $N(\mu = 0, \sigma = 15)$ is added that has a mean $\mu = 0$ and a standard deviation $\sigma = 15$ cm s^{-1}. The signal-to-noise ratio is thus $O(1)$.

b. Test statistics and errors

In order to estimate errors, I use the location and time (x, y, z, t) of the actual measurements to prescribe the velocity field according to (9) and (10). The least squares fit to these ''artificial'' data results in a set of coefficients α_{jk} and β_{jk} that are then used to predict a velocity field at discrete grid locations using (5). Next I compare the ''predicted'' velocity field [(5)] with the ''known'' velocity field [(9)]. At the grid locations shown in Fig. 1a, the rms discrepancy between the predicted and the known velocity constitutes a test statistic that in Table 3 is termed ''grid error.'' It measures the performance of the spatial interpolation on a uniform grid without reference to the measurement locations. In order to estimate the method's performance at measurement locations only, I define a second test statistic as the rms between predicted and known velocity at data sampling locations. In Table 3 it is termed ''data error.''

Figure 4 shows a visual example of the test statistic grid error. The right panels of Fig. 4 show the amplitude of the simulated M_2 tidal velocity fields that have uniform gradients in both the north–south and vertical directions. The noise component is not shown, but the left panels quantify the grid error as a function (x, y, z). The global grid error listed in Table 3 is 2.7 cm s^{-1} for this case, with a standard deviation of 2.3 cm s^{-1}. The mean and standard deviation (i.e., 2.7 ± 2.3 cm s^{-1}) are determined from velocities on a $6 \times 6 \times 6$ grid in three spatial dimensions. The largest errors occur at locations where the method extrapolates. In contrast, errors are generally smaller than 2 cm s^{-1}, where the method interpolates. This is also reflected in the much smaller data error; that is, the along-track rms velocity errors are 1.9 and 0.5 cm s^{-1} in the u and v components, respectively. Recall from (9) and (10) that only the u component contains a tidal signal, while both components contain noise with an rms of 15 cm s^{-1}. The capability of the method to resolve both horizontal and vertical tidal current shear in the presence of noise is encouraging.

c. Sensitivities using equally weighted data

The standard case 1 uses data from moorings and ADCP surveys along with six nodal locations (shown in Fig. 5) to predict M_2 and K_1 tidal currents. The grid error is about 20% smaller than that shown in Fig. 4 (Table 3). The solution changes little if I remove the C2 mooring data from the interpolation (case 1a). Since the amount of ADCP survey and OSCR data is large, only a randomly selected subset of these data (10% of the ADCP survey) is used. Increasing the amount of the ADCP survey data by a factor of 2 does not affect the solution (case 1b), but using additional ADCP survey data preferentially from offshore locations degrades the fit (case 1c) because the spatial sampling offshore does not resolve the Nyquist frequency properly. The use of only mooring data eliminates this spatial sampling error and generally results in ''good'' solutions (cases 1d and 8d). However, the method then merely extrapolates results from mooring locations to offshore. The use of additional OSCR data degrades the fit also (case 1e). The OSCR data are all at the surface and, if given equal weight, bias smaller tidal currents at depth toward larger surface values.

The solutions are most sensitive to the location of the nodes. Holding the horizontal locations of the nodes fixed, I varied the vertical locations slightly in cases 2–6 (Table 3). The change of a single nodal location from 0.25 to 0.50 to 0.75 in the vertical does not affect the solution significantly; however, changing the pattern systematically such that all deep nodes are offshore and all shallow nodes are inshore (case 4) does. The actual location of the vertical nodes, too, can change the solution dramatically (cases 5 and 6). This finding emphasizes the need to carefully test each configuration of nodes before it is applied to actual data.

Cases 7–9e demonstrate that similar results can be obtained with both a different set of nodes and different record lengths. Cases 7 and 9 fit tides to the entire 60-day-long record, while case 8 fits tides only to a 7-day-long subset. The results are encouraging. First, the errors of cases 7 are similar to the errors of cases 1, even though the horizontal and vertical node locations are very different. Second, the errors of shorter records are similar to those of longer records (cases 7 versus cases

TABLE 3. Test cases and statistics. The labels M, A, and O represent mooring, ADCP survey, and OSCR data, respectively. The horizontal node locations for cases 1–6 are shown in Fig. 4, while those for cases 7–9 are shown in Fig. 5. The *z* nodes refer to vertical locations of the nodes. All data are weighted equally except in case 9. The labels *K* and *M* for columns 3 and 4 indicate the number of nodes and tidal constituents, respectively.

Case	Data	*K*	*M*	Grid error (cm s^{-1})	Data error *u*/*v* (cm s^{-1})	Comments
1	M + A	6	2	2.2 ± 1.8	1.3/0.5	*z* nodes: 0.25/0.75/0.75/0.25/0.75/0.25 (see Fig. 4)
1a	M + A	6	2	2.1 ± 1.4	1.6/0.5	As in case 1 but without data from the C2 mooring
1b	M + A	6	2	2.2 ± 1.6	1.6/0.6	As in case 1a but with twice the amount of ADCP survey data
1c	M + A	6	2	2.9 ± 2.4	2.1/0.5	As in case 1 but with more offshore ADCP survey data
1d	M	6	2	2.2 ± 1.2	1.8/0.7	As in case 1a but with only mooring data
1e	M + A + O	6	2	2.4 ± 0.8	2.0/0.8	As in case 1a but with additional OSCR data
1f	M + A	6	4	4.7 ± 3.7	4.1/0.7	As in case 1a but with four tidal constituents
2	M + A	6	2	2.1 ± 1.4	1.6/0.5	*z* nodes: 0.75/0.25/0.25/0.75/0.25/0.75
3	M + A	6	2	2.0 ± 1.3	1.3/0.5	*z* nodes: 0.50/0.25/0.75/0.75/0.25/0.75
4	M + A	6	2	8.3 ± 26.1	7.3/0.8	*z* nodes: 0.75/0.25/0.75/0.25/0.75/0.25
5	M + A	6	2	4.8 ± 1.3	3.6/2.2	*z* nodes: 0.35/0.65/0.65/0.35/0.65/0.35
6	M + A	6	2	9.8 ± 5.4	6.8/3.3	*z* nodes: 0.15/0.85/0.85/0.15/0.85/0.15
7	M + A	5	2	2.8 ± 2.2	2.0/0.5	Three horizontal node locations (see Fig. 5)
7a	M + A	5	4	4.9 ± 4.4	3.5/0.9	As in case 7 but four with tidal constituents
8	M + A	5	2	3.1 ± 2.0	2.1/0.8	As in case 7 using a 7-day record with 27% ADCP survey and 73% mooring data (near spring tide)
8a	M + A	5	2	3.4 ± 3.2	2.5/1.0	As in case 8 but for a 7-day period (near neap tide)
8b	M + A	5	2	3.2 ± 1.7	2.5/0.7	As in case 8 but with a 39% ADCP survey and 61% mooring data
8c	M + A	5	2	3.5 ± 1.9	2.6/0.7	As in case 8 but with a 54% ADCP survey and 46% mooring data
8d	M	5	2	5.2 ± 6.7	2.7/1.4	As in case 8 but with mooring data only
8e	M + A + O	5	2	4.4 ± 2.5	2.9/2.4	As in case 8 but with 17% OSCR, 22% ADCP survey, and 61% mooring data
8f	A	5	2	17.6 ± 30.9	11.6/6.3	As in case 8 but with 4364 ADCP data only
8g	A	5	2	14.9 ± 5.7	9.9/6.5	As in case 8 but with 9752 ADCP data only
9	M	5	4	3.5 ± 2.3	2.0/0.9	Similar to case 7a but with 12 707 mooring data
9a	M + A	5	4	7.0 ± 13.0	4.8/0.6	As in case 9 but with additional 10 213 ADCP data
9b	M + A	5	4	3.7 ± 2.1	2.4/0.7	As in case 9a but with error 1 (mooring) and 5 (ADCP)
9c	M + A + O	5	4	3.4 ± 2.3	2.1/0.6	As in case 9a but with additional 6089 OSCR data with error 10
9d	M + A + O	5	4	3.4 ± 1.9	2.2/0.6	As in case 9c but with 14 428 ADCP and 10 176 OSCR data (same weights)
9e	M + A + O	5	2	2.7 ± 2.4	1.9/0.5	As in case 9d but for two tidal constituents only

8). Third, the sensitivity to changes in parameters and input data distributions are all similar to the sensitivities of cases 1. It is not possible, however, to reliably estimate tidal currents from the ADCP survey data alone (cases 8f and 8g). The three-dimensional spline interpolation of this study thus requires both mooring and ADCP survey data to predict tidal currents within rms errors of less than 4 cm s^{-1}.

In cases 1f and 7, the number of tidal constituents *M* is increased from 2 (M_2 and K_1) to 4 (M_2, K_1, N_2, and O_1). The uncertainty increases with each coefficient because the solution depends on the inversion of the $4KM \times 4KM$ matrix. Here *M* and *K* are the number of tidal constituents and nodes, respectively. The condition of the matrix degrades as the ratio of its smallest to its largest eigenvalue becomes small (Candela et al. 1992). For cases that use $M = 2$ and $K < 7$, this condition number is less than 10^{-3}. Hence, all matrix inversions with $M = 2$ are very stable, while matrix inversions using $M = 4$ are less stable. The added uncertainty for cases with $M = 4$ thus must be compared against the actual contribution of the neap–spring cycle to the tidal variability in a given study area at a given time. For the study area off New Jersey, in 1996, resolution of the small spring–neap cycle requires properly weighted data from several platforms.

d. Sensitivity using unequally weighted data

Velocity data from diverse sources such as moorings, ADCP surveys, and OSCR deployments all have different measurement errors. The least squares methods in this section reflect these uncertainties through weights assigned to the velocity data from different platforms. The weights used are the inverse of their errors; that is, the σ_i in (7) are interpreted as relative errors. More specifically, relative errors σ_i of 1 cm s^{-1} are assigned to all mooring data, of 5 cm s^{-1} to all ADCP survey data, and of 10 cm s^{-1} to all OSCR data.

Cases 9–9e use the same record length and nodes as

case 7. Fitting only mooring data to four tidal constituents (M_2, N_2, K_1, and O_1), I find a grid error of 3.5 $\pm$ 2.3 cm s^{-1} (case 9, Table 3). The error doubles to an unacceptable 7.0 $\pm$ 13.0 cm s^{-1} when a roughly equal number of ADCP survey data are also included in the fit with equal weight (case 9a). However, by assigning the unequal weights for mooring and ADCP survey data, a more reasonable grid error of 3.7 $\pm$ 2.1 cm s^{-1} results (case 9b). The fit further improves with the inclusion of additional OSCR and ADCP data (case 9d). That is, the grid error is now down to 3.4 $\pm$ 1.9 cm s^{-1}. The data error is less than 2 cm s^{-1}, even though many more measurement locations are included in case 9d as compared to case 9. I thus conclude that, at the 1996 measurement locations, it is possible with the data and method on hand to predict combined currents from two semidiurnal and two diurnal constituents with an rms of better than 2 cm s^{-1}. This does not imply—I emphasize—that all details of all constituents are predicted equally well at all locations. The fit and stated accuracies are purely statistical, and no physical significance should be attached to them. Furthermore, there are locations where discrepancies can reach 7 cm s^{-1} within a 95% confidence limit. As demonstrated herein, however, these large errors occur more than 15 km beyond the edges of the 1996 measurement locations.

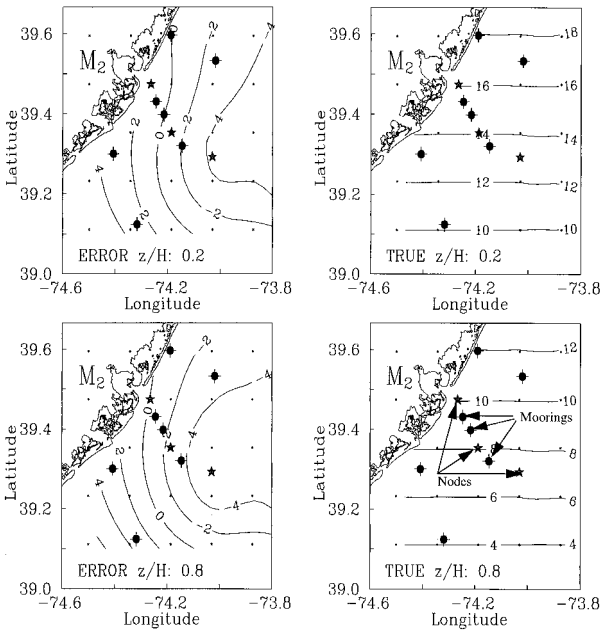

FIG. 4. Maps of the semimajor axes (RMAJ) of the artificial M_2 tidal current field (right panel) and the absolute error (left panel) in predicting this major axis near the surface ($z/H = 0.2$) and bottom ($z/H = 0.8$) for case 9e (Table 3). Also shown are the node (stars) and mooring locations (crossed circles) used in the least squares fit. The small dots indicate grid locations (see Fig. 1a) used to estimate error statistics.

e. Summary

The arbitrary choice of nodal locations represents the single most serious drawback of the biharmonic spline interpolation technique. The analyst must carefully test the performance of a particular set of nodal locations for each application. The sensitivity of the data distribution to nodal locations, too, must be investigated in each application. This drawback neither invalidates nor does it recommend the method for casual use, but the same probably applies to any detiding method. Provided a good solution is found (such as cases 1, 7, 8, and 9d), the algebraic expression containing 2*KM* coefficients for each velocity component provides predictions of overall tidal currents to within 3.5 cm s^{-1} rms. The simplicity of this ''prediction'' is the main advantage of the empirical over the numerical detiding method (Candela 1992; Münchow et al. 1992; Allen 1995; Steger et al. 1998). Weighted least squares methods that use a variety of data from different sources perform better than methods that use only equally weighted data.

6. Verification

In order to verify the least squares solution, tidal predictions were compared against velocity measurements that were not used in the least squares procedure. More specifically, in this section, maps of predicted and observed tidal ellipses at two different depths are compared first (Fig. 5, case 3, Table 3). Subsequently, I discuss absolute errors as a function of time at a single 1984 (Fig. 6) and 1996 (Fig. 7) mooring location that use the algorithm of case 9e and case 9d, respectively. Finally, Figs. 8 and 9 compare vertical profiles of ellipse parameters predicted with those observed at C2 (Fig. 3).

Figure 5 shows M_2 and K_1 tidal ellipses near the surface and bottom from both a biharmonic spline prediction (case 3, Table 3) and observations at mooring locations. The velocity field for the semidiurnal M_2 tide varies from less than 5 cm s^{-1} in the northwest to more than 15 cm s^{-1} in the southeast. The major axes are oriented dominantly across the shelf with sizable minor axes. Currents generally rotate clockwise (not shown) and are overall in phase within about 30° or 1 h (not shown). The M_2 tide is largely barotropic, with some vertical variation in ellipse parameters due to bottom friction. The ellipse parameters agree with the analytical solutions of Battisti and Clarke (1982) and with the observations of Münchow et al. (1992b). Diurnal tidal currents exhibit a different pattern. While their amplitudes are smaller—about 2–4 cm s^{-1}—their orientation in the summer of 1996 varies from across shore near the surface to generally alongshore at depth. The minor axes are either small or vanish. Hence, K_1 tidal currents are rectilinear.

Figure 6 shows the difference between the observed and predicted tidal currents near the surface for NOS mooring location 24. A two-week-long time series of the east and north component of the observed tidal flow is

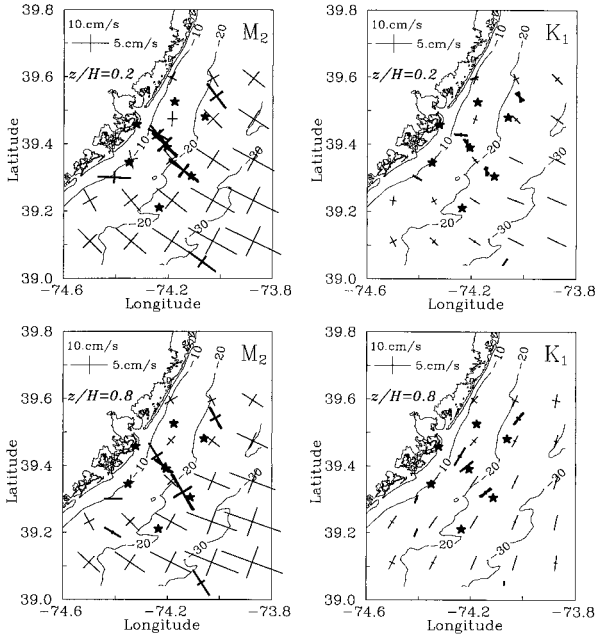

FIG. 5. Maps of the magnitude and orientation of semimajor (RMAJ) and semiminor (RMIN) axes of the M_2 (left panel) and the K_1 (right panel) tidal ellipse for case 3. The depth levels $z/H = 0.2$ and $z/H = 0.8$ represent near-surface and near-bottom currents, respectively. Contours represent the bottom topography from the 10-m to the 30-m isobath. Ellipses in bold font are from moorings. Stars indicate the horizontal locations of the six nodes used in the least squares fit. Note that the observed M_2 tidal ellipses at the mooring location N1 (see Fig. 1b for location) are invisible as RMAJ is less than 2 cm s^{-1} there.

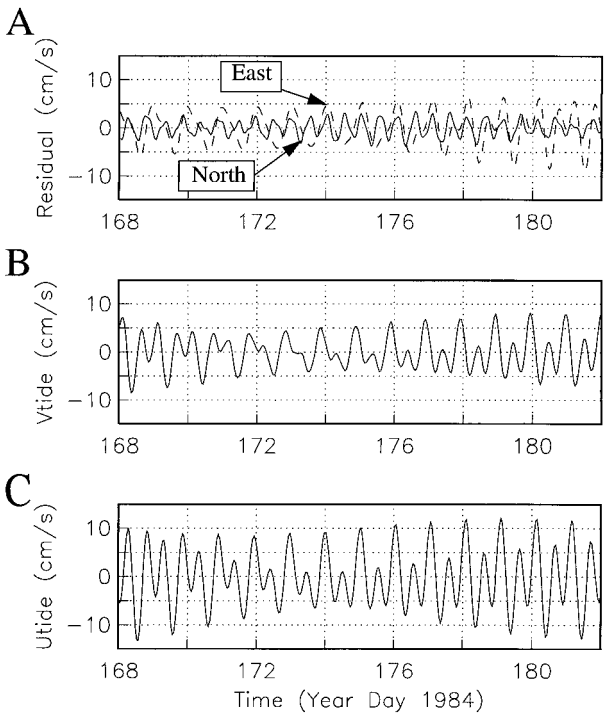

FIG. 6. Two-week-long time series of (a) tidal prediction error (residual), (b) observed north (Vtide), and (c) observed east (Utide) component of the $M_2 + N_2 + K_1 + O_1$ tidal velocity. The data are from the middepth instrument at NOS mooring 24 deployed in the summer of 1984 on the 18-m isobath at the southern edge of the study area (see Fig. 1b for location). Tidal prediction uses case 9e (Table 3).

shown also for comparison. The instantaneous error is less than 5 cm s^{-1} in both components. The tidal amplitude of the error varies from about 4 cm s^{-1} near day 173 to 6 cm s^{-1} seven days later. The error in the east–west component (across shore) is largely diurnal, while the error is semidiurnal for the north–south component (along shore). The amplitude of the error is modulated only weakly during a fortnightly period. This suggests that the unresolved spring–neap cycle causes only small errors at this location. Nevertheless, the rms error is only 3.5 cm s^{-1}, and thus, contrasts to the much larger errors at the offshore location 25 (not shown), where the rms error reaches 7 cm s^{-1}, almost as large as the tidal signal itself. Note, however, that the offshore mooring 25 is 15 km offshore of the study area: that is, the method extrapolates. In contrast, the inshore mooring location 24 skirts the southern leg of the 1996 ADCP survey leg. Furthermore, it is located roughly halfway between the 1996 mooring locations S1 and S3, where the rms error varies between 3 and 5 cm s^{-1}. The rms errors at the 1984 and, as demonstrated next, the 1996 mooring locations change little if the neap–spring cycle is resolved.

A second independent verification of the least squares tidal prediction uses high-resolution 1996 ADCP data at C2. Figure 1b shows its location at the center of the study area, Fig. 3 depicts its observed ellipse parameters, and Fig. 7 presents time series of the misfit error at three different depths using case 9d for detiding. Similar to Fig. 6a, the misfit constitutes an absolute error. It rarely exceeds 5 cm s^{-1}. Root-mean-square errors are 4.7, 3.1, and 3.2 cm s^{-1} near the surface (Fig. 7a), at middepth (Fig. 7b), and near the bottom (Fig. 7c), respectively. These errors for a mooring deployed in 1996 at the center of the array are similar to the errors shown in Fig. 6a for a mooring deployed in 1984 at the edge of the array. The neap–spring cycle is resolved. However, the errors nevertheless exhibit weak fortnightly variability that indicates small inadequacies with which the two semidiurnal constituents are resolved. Hence, little is gained by the inclusion of the additional two tidal coefficients off New Jersey.

In summary, the biharmonic spline interpolation succeeds in predicting tidal currents throughout the study area to within an rms error of generally less than 4 cm s^{-1}. This success does not imply, however, that the resulting vertical profiles of tidal ellipse parameters are always reasonable. As a note of caution, Figs. 8 and 9 compare the predicted vertical profiles of tidal ellipse parameters at C2 for both the M_2 and the K_1 currents, respectively. Note especially the large 5 cm s^{-1} discrepancy in the prediction of the M_2 amplitude along the semimajor axis RMAJ near the surface. This large

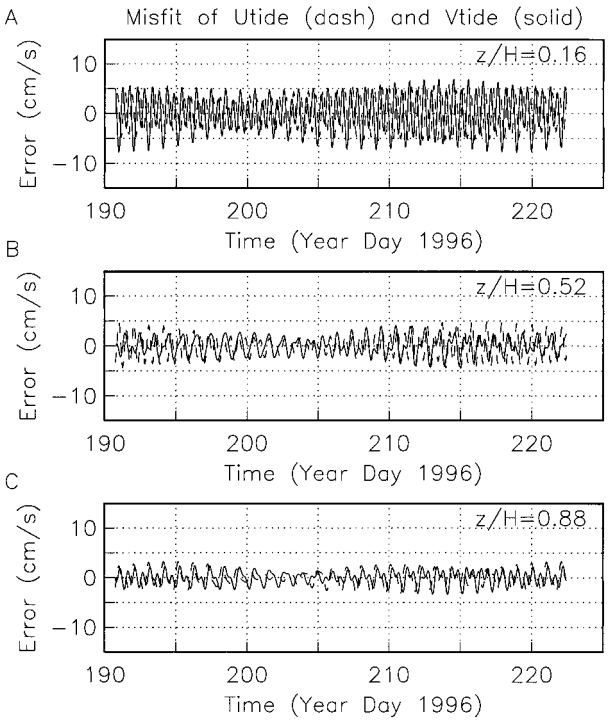

FIG. 7. Time series of tidal prediction error at C2 for (a) $z/H = 0.16$ (near surface), (b) $z/H = 0.52$ (middepth), and (c) $z/H = 0.88$ using algorithm and data from case 9d (Table 3). The prediction errors can be compared with similar errors shown in Fig. 6a for the 1984 NOS 24 at the southern edge of the 1996 study area (see Fig. 1b for locations).

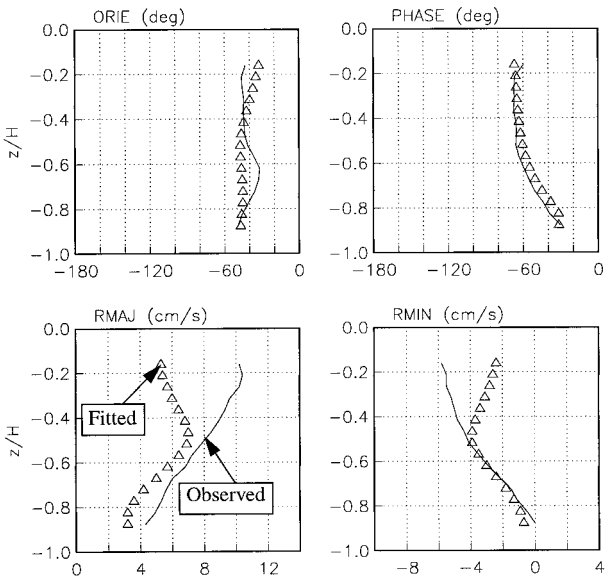

FIG. 8. Comparison of vertical profiles of observed (solid line) and predicted (triangles) tidal ellipse parameters for the M_2 constituent at mooring C2 using case 9d.

error is compensated partly by a similarly large discrepancy of the semiminor axis RMIN and partly by a discrepancy near the surface in K_1 semimajor axes orientation (ORIE) and phase (PHASE). Note, however, the near-perfect match of both M_2 tidal phase and major axes orientation. The tidal prediction also reproduces the K_1 amplitudes of the semimajor and semiminor axes at all depth. Hence, the physically accurate detiding of coastal ADCP records in all three dimensions is still a problem to be solved. I merely suggest a pragmatic approach to reduce tidal variance that varies substantially in all three spatial dimensions.

7. Application

The main purpose of this study is to demonstrate and to quantify errors associated with a new method that removes tidal currents in all three spatial dimensions from ADCP survey data. The least squares biharmonic spline fit results in a closed algebraic expression for the tidal currents as a function of (x, y, z, t). It is straightforward and efficient to incorporate this prediction into real-time velocity data collection efforts. The ease of implementation and application of the method is its major advantage over more sophisticated methods that rely on numerical simulations. Now a short velocity record is used from an ADCP–CTD survey of the inner New Jersey shelf, which was conducted in August 1996. The raw velocity time series 6.5 m below the surface shows large fluctuations (Fig. 10a) that could have been caused by either temporal or spatial variability of either the tidal or the subtidal velocity fields. Figure 11a shows the same fields as a map. Without a thoroughly tested detiding method, it is impossible to interpret this record properly. Note the large across-shore velocities that on shallow and broad continental shelves are often associated with tidal currents (Battisti and Clarke 1984;

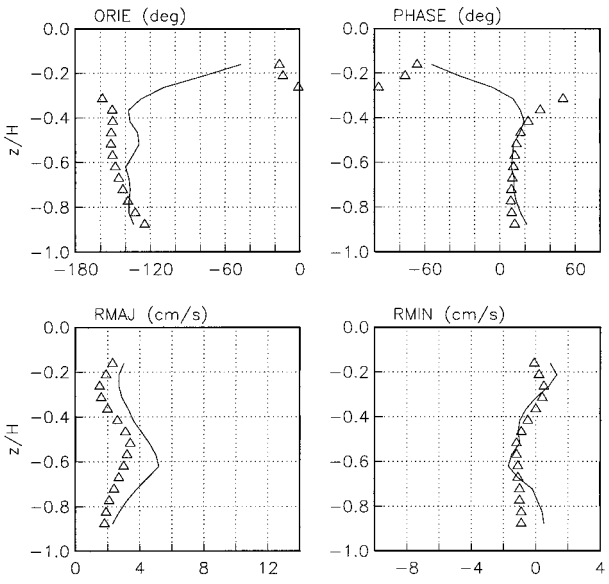

FIG. 9. As in Fig. 8 but for the K_1 constituent at mooring C2.

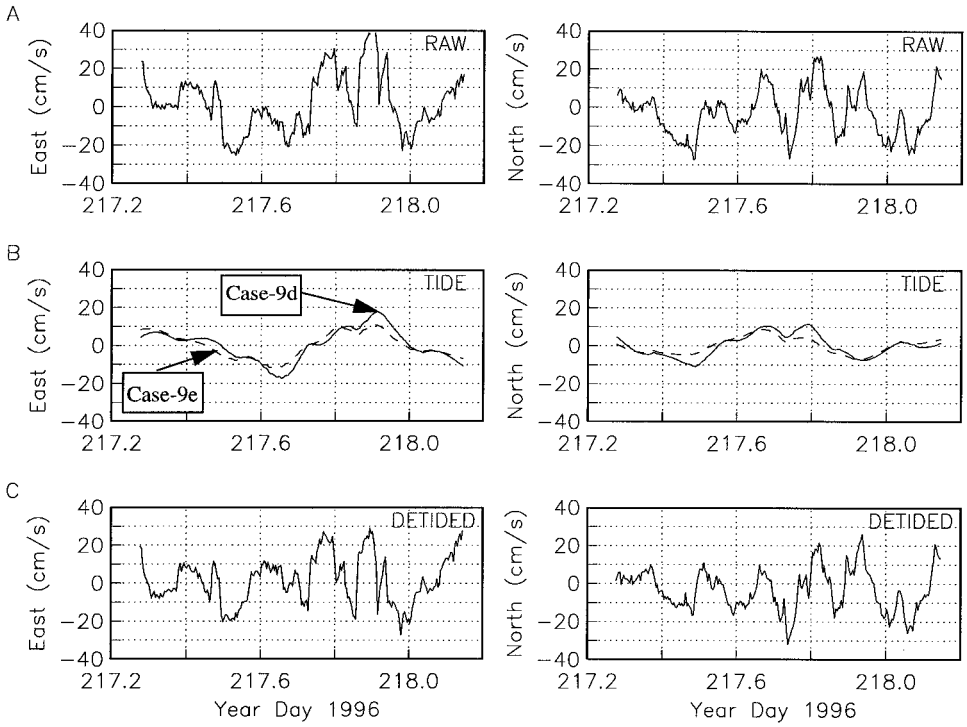

FIG. 10. Time series of (a) raw ADCP survey data collected at ($t, x, y, z = 6.5$ m), (b) tidal predictions at ($t, x, y, z = 5$ m) from case 9d (M_2, K_1 N_2, and O_1; solid line) and case 9e (M_2 and K_1; dashed line), and (c) the detided currents (case 9d) that are the difference between (a) and (b). The left and right panels show east and north components of the velocity vectors. The data are also shown in Figs. 11a (raw), 11b (detided), and 11e (tides).

Münchow et al. 1992b). The tidal predictions (case 9d) shown in Figs. 10b and 11e, however, reveal that the tidal currents are rather weak relative to the residual currents shown in Figs. 10c and 11b. The residual detided currents are the difference between the raw currents and the predicted tidal currents (Fig. 11).

Figure 11 also includes vector maps at 16.5 m below the surface. The flow field appears strongly surface intensified at subtidal frequencies. The tidal currents at the surface are only about 20% of the detided currents (Fig. 11e). In contrast, tidal currents at depth are of similar magnitude as the detided currents. (Note that the scale of the tidal currents in Fig. 11 is a factor of 2 larger than the scale for the raw and detided currents.) The apparent baroclinicity of the flow is particularly strong in the northern part of the study area, where the buoyancy-driven Hudson Coastal Current dominates the surface circulation. Yankovsky et al. (1999, manuscript submitted to *J. Phys. Oceanogr.*) discuss and interpret the detided velocity fields such as those shown in Fig. 11c. They attribute the large across-shore velocities to the nose of the Hudson Coastal Current that passed through the study area at the time of the survey. The frontal passage and associated baroclinic flow field are both unsteady and spatially variable (Yankovsky et al. 1999, manuscript submitted to *J. Phys. Oceanogr.*).

8. Conclusions

A statistical method to remove tidal currents from shipborne velocity surveys was thoroughly tested. The method extends previous work by Candela et al. (1992) from two to three spatial dimensions. Biharmonic splines are fitted by the method of least squares to construct smoothly varying semidiurnal and diurnal tidal current fields in all three spatial dimensions. These fields are determined using current measurements from moorings, ADCP surveys, and surface current radar. Extensive testing of the method against synthetic data with known signal and noise properties reveals that the method predicts tidal currents to within better than 4 cm s^{-1} in a tidal field with amplitudes of about 20 cm s^{-1} and noise of similar magnitude. Absolute error estimates result if current predictions are compared against independent mooring data that were not included in the fitting procedure. Mooring data from both 1984 and 1996 are predicted equally well by the fit eventually adopted (case 9d). Furthermore, I find little difference in the skill of the prediction using a number of different variations of data input and model parameters detailed in Table 3. Thus, the adopted least squares ''solution'' (case 9d) is both robust and reasonably accurate to remove tidal currents from shipborne surveys of the study area off New Jersey. It is accurate to within better than 3.5 cm s^{-1} rms. This does not imply that all details of

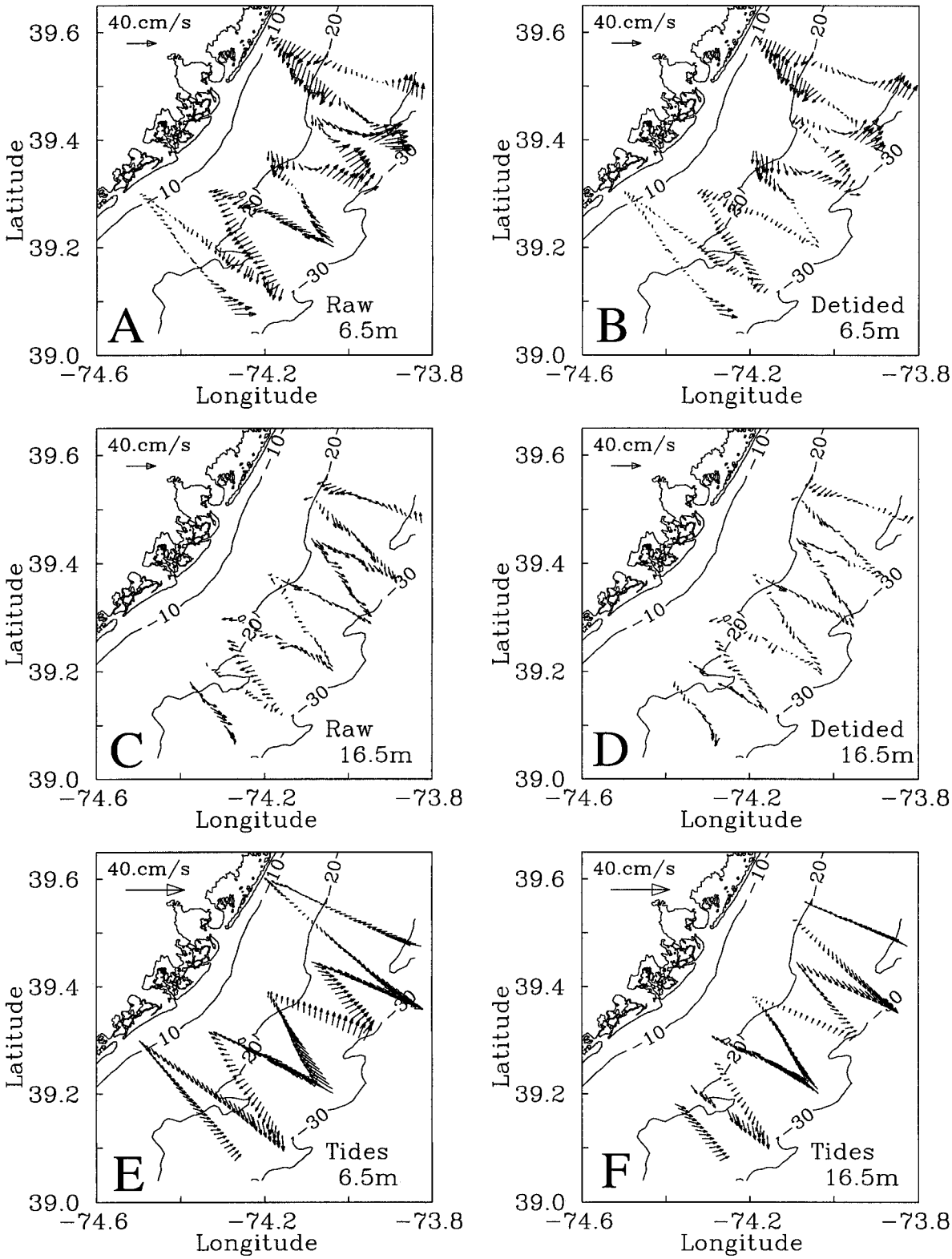

FIG. 11. Map of current vectors of (a) raw and (b) detided ADCP survey data collected at 6.5 m; (c) raw and (d) detided ADCP survey data at 16.5-m depth; and, with a different velocity scale, tidal predictions at (e) 6.5-m and (f) 16.5-m depth. The tidal predictions are from case 9d. The detided currents result after the tidal currents are removed from the raw data. The data in (a), (b), and (e) are identical to those shown as (solid line) time series in Figs. 10a, 10b, and 10c, respectively. Contours are depth contours.

every constituent and every ellipse parameter are predicted equally well. Nor does it imply that all locations are fitted equally well. Recall that the spatially mean grid error for the adopted case 9d has a standard deviation of 1.9 cm s^{-1}; that is, a rough estimate of an upper bound at a 95% confidence level is approximately 8 cm s^{-1}. Verification of the method against mooring data at a variety of locations indicates, however, that this upper bound is realized only more than 15 km beyond the outer edges of the 1996 study area. Within the study area where the method largely interpolates, uncertainties are much closer and often substantially below the mean rms grid error of 3.4 cm s^{-1}.

The biharmonic spline interpolation to the data reveals physically consistent tidal velocity fields. While some details of the predicted tidal fields agree well with theoretical and observational expectations, other details are purely statistical. Main features of the semidiurnal tidal currents, such as the clockwise rotation of currents and a major axis oriented across the shelf, are well resolved. The proposed new detiding method thus appears broadly reasonable but nevertheless constitutes a statistical fit only. The physical misfit in one tidal ellipse parameter generally is compensated by a similar physical misfit in another ellipse parameter of the same or a different tidal constituent. Expressed differently, the problem of statistically detiding shipborne ADCP records to within an absolute error of about 5 cm s^{-1} (or an rms error of about 3 cm s^{-1}) is within reach. However, physically consistent detiding of coastal ADCP records in all three dimensions to the same degree of accuracy is still a challenge to be met.

Acknowledgments. The experiment was a joint effort with Richard Garvine of the University of Delaware and Scott Glenn of Rutgers University (RU). The competent mooring work was conducted by divers and shipboard personnel of both universities. I thank both Sasha Yankovsky (Nova Southeastern University) and Robert Chant (RU) for numerous enlightening conversations and for initially processing mooring, ADCP, and OSCR data with me. James O'Donnell of the University of Connecticut and Eddy Carmack of the Canadian Institute of Ocean Sciences kindly loaned me their ADCPs for survey and mooring deployments, respectively. Hans Graber of Miami University provided the OSCR unit, and his group assisted in its operation in the field. Comments and challenging questions by Rich Garvine, Sasha Yankovsky, and an anonymous reviewer encouraged this study and improved an early draft. Data and software are accessible through the World Wide Web at http://marine.rutgers.edu/ac/data.html. The National Science Foundation funded this study through Grants OCE-95-28239 and OPP-97-08349.

REFERENCES

Allen, J. T., 1995: Subtidal and tidal currents in the vicinity of the Iceland–Færæs front. *J. Atmos. Oceanic Technol.,* **12,** 567–588.

Battisti, D. S., and A. J. Clarke, 1982: A simple method for estimating barotropic tidal currents on continental margins with specific applications to the M_2 tide off the Atlantic and Pacific coasts of the United States. *J. Phys. Oceanogr.,* **12,** 8–16.

Bogden, P. S., and J. O'Donnell, 1998: Generalized inverse of ship-board current measurements: Tidal and non-tidal flows in Long Island Sound: *J. Mar. Res.,* **56,** 995–1027.

Candela, J., R. C. Beardsley, and R. Limeburner, 1992: Separation of tidal and subtidal currents in ship-mounted acoustic Doppler current profilers. *J. Geophys. Res.,* **97,** 769–788.

Dowd, M., and K. R. Thompson, 1996: Extraction of tidal streams from a ship-borne acoustic Doppler current profiler using a statistical–dynamical model. *J. Geophys. Res.,* **101,** 8943–8956.

Foreman, M. G. G., and H. J. Freeland, 1991: A comparison of techniques for tide removal from ship-mounted acoustic Doppler measurements along the southwest coast of Vancouver Island. *J. Geophys. Res.,* **96,** 17 007–17 021.

Geyer, R., and R. Signell, 1990: Tidal flow measurements around a headland with shipboard acoustic Doppler current profiler. *J. Geophys. Res.,* **95,** 3189–3197.

Joyce, T. M., 1989: On in situ ''calibration'' of shipboard ADCPs. *J. Atmos. Oceanic Technol.,* **6,** 169–172.

——, and M. C. Stalcup, 1984: An upper ocean current jet and internal waves in the Gulf Stream warm core ring. *J. Geophys. Res.,* **89,** 1997–2003.

Kaneko, A., W. Koterayama, H. Honji, S. Mizuno, K. Kawatate, and R. L. Gordon, 1990: Cross-stream survey of the upper 400 m of the Kuroshio by an ADCP on a towed fish. *Deep-Sea Res.,* **37,** 875–889.

Kosro, P. M., and A. Huyer, 1986: CTD and velocity surveys of seaward jets off northern California, July 1981 and 1982. *J. Geophys. Res.,* **91,** 7680–7690.

Maas, L. R. M., and J. J. M. Van Haren, 1987: Observations on the vertical structure of tidal and inertial currents in the central North Sea. *J. Mar. Res.,* **45,** 293–318.

McIntosh, P. C., 1990: Oceanographic data interpolation: Objective analysis and splines. *J. Geophys. Res.,* **95,** 13 529–13 541.

Münchow, A., and R. J. Chant, 2000: Kinematics of inner shelf motions during the summer stratified season off New Jersey. *J. Phys. Oceanogr.,* **30,** 247–268.

——, R. W. Garvine, and T. F. Pfeiffer, 1992a: Subtidal currents from a shipboard acoustic Doppler current profiler in tidally dominated waters. *Contin. Shelf Res.,* **12,** 499–515.

——, A. K. Masse, and R. W. Garvine, 1992b: Astronomical and nonlinear tidal currents in a coupled estuary shelf system. *Contin. Shelf Res.,* **12,** 471–498.

——, C. S. Coughran, M. C. Hendershott, and C. D. Winant, 1995: Performance and calibration of an acoustic Doppler current profiler towed below the surface. *J. Atmos. Oceanic Technol.,* **12,** 435–444.

Prandle, D., 1982: The vertical structure of tidal currents. *Geophys. Astrophys. Fluid Dyn.,* **22,** 22–49.

Press, W. H., S. A. Teukolsky, W. T. Vetterling, and B. P. Flannery, 1992: *Numerical Recipes in Fortran 77.* 2d ed. Cambridge University Press, 933 pp.

Ray, R. D., and G. T. Mitchum, 1996: Surface manifestations of internal tides generated near Hawaii. *Geophys. Res. Lett.,* **23,** 2101–2104.

Regier, L., 1982: Mesoscale current fields observed with a shipboard profiling acoustic current meter. *J. Phys. Oceanogr.,* **12,** 880–886.

Sandwell, D. T., 1987: Biharmonic spline interpolation of *GEOS-3* and SEASAT altimeter data. *Geophys. Res. Lett.,* **14,** 139–142.

Steger, J. M., C. A. Collins, F. B. Schwing, M. Noble, N. Garfield, and M. T. Steiner, 1998: An empirical model of the tidal currents in the Gulf of Farallones. *Deep-Sea Res. II,* **45,** 1471–1505.

Yankovsky, A. E., and R. W. Garvine, 1998: Subinertial dynamics on the inner New Jersey shelf during the upwelling season. *J. Phys. Oceanogr.,* **28,** 2444–2458.